14 April 2000

ELSEVIER

Chemical Physics Letters 320 (2000) 499–506

CHEMICAL PHYSICS LETTERS

www.elsevier.nl/locate/cplett

A combined experimental and theoretical study of resonance emission spectra of $SO_2(\tilde{C}\,^1B_2)$

Brad Parsons [a], Laurie J. Butler [a,1], Daiqian Xie [b,2], Hua Guo [b,*]

[a] *The James Franck Institute and the Department of Chemistry, University of Chicago, Chicago, IL 60637, USA*
[b] *Department of Chemistry, University of New Mexico, Albuquerque, NM 87131-1096, USA*

Received 12 October 1999; in final form 24 February 2000

Abstract

Experimental and theoretical resonance emission spectra are obtained for a number of vibrational states of $SO_2(\tilde{C}\,^1B_2)$. The experimental emission spectra are dominated by $(n_1\nu_1, n_2\nu_2, 0)$ bands, but some weak activity in the anti-symmetric stretch (ν_3) is observed. The calculated emission spectra based on an empirical near-equilibrium potential energy surface agree reasonably well with experiment for two lowest states investigated here, but fail to reproduce higher ones. Resonance Raman spectra are also calculated and agree well with an earlier experiment.

1. Introduction

It is well-known that the $\tilde{C}\,^1B_2$ state of SO_2 is predissociative at wavelengths shorter than 219 nm, as manifested spectroscopically by an abrupt drop in fluorescence yield [1–6]. Interestingly, the predissociation threshold coincides with the dissociation energy (D_0) of the ground $(\tilde{X}\,^1A_1)$ electronic state, which has been measured accurately (45 725.3 cm^{-1} or 218 nm) [7]. The decay of fluorescence yield is nearly exponentially proportional to the excess energy [5,6], although some mode specificity involving the anti-symmetric stretch (ν_3) has been observed [3,5,6,8,9]. Dynamically, the dissociation products, $SO(^3\Sigma^-) + O(^3P)$, have been measured using various experimental techniques between 218 and 193 nm [7,10–15].

Although the existence of non-adiabatic interactions between the $\tilde{C}^1B_2$ and nearby electronic states is well-established, the detailed predissociation mechanism is not yet completely understood. Near 193 nm, experimental [10–13] and theoretical [6,16] evidence supports the involvement of a repulsive state, which intersects with the bound $\tilde{C}^1B_2$ state at large S–O distances. Kanomori et al. [12] identified it as a repulsive triplet state, but recent emission spectroscopy work [17] indicates the involvement of a repulsive singlet A_1 state in the predissociation at

* Corresponding author. Fax: +1-505-2772609; e-mail: hguo@unm.edu
[1] Also corresponding author. Fax: +1-773-7025863; e-mail: ljb4@midway.uchicago.edu.
[2] Visiting Professor, Permanent address: Department of Chemistry, Sichuan University, Chengdu, Sichuan, P.R. China.

0009-2614/00/$ - see front matter
PII: S0009-2614(00)00253-0

C_s geometries near 50 000 cm^{-1}. Ab initio calculations [6,16,18] confirmed the intersection of the $\tilde{C}\,^1B_2$ state with both triplet and singlet states at respectively 6700 and 9700 cm^{-1} above the dissociation limit [6]. Near the predissociation threshold, however, the process seems to follow a different pathway. Ivanco et al. [9] suggested that the dynamics is via internal conversion to the state $\tilde{X}$, followed by prompt dissociation. This mechanism is supported by the observed exponential decrease of fluorescence yield with the excess energy [5,6] and statistical energy disposal in the products [7,15], and consistent with the observation that the ν_3 vibration is the promoting mode [5,9]. The two predissociation pathways may coexist with each dominating in different energy ranges [6].

Dispersed resonance emission and resonance Raman experiments via the $\tilde{C}\,^1B_2$ state have been reported in both gas [17,19–22] and condensed phases [22]. Emission from the bottom of the $\tilde{C}\,^1B_2$ state potential energy surface provides information on highly excited vibrational levels in the $\tilde{X}\,^1A_1$ state [20,21], which are difficult to access otherwise. Ray et al. [17] have recently reported a resonance emission study of $SO_2(\tilde{C}\,^1B_2)$ near 200 nm. They observed strong transitions to states with odd quanta in ν_3 the anti-symmetric stretching mode. Some activity in odd ν_3 was noted in earlier emission studies [19,22], but attributed to *c*-axis Coriolis coupling. Since such transitions are symmetry forbidden if the excited electronic state is of pure $^1B_2$ character, the appearance of strong emission bands into states with odd quanta in was interpreted by Ray et al. [17] as an indication that the $\tilde{C}\,^1B_2$ state is strongly mixed with a $^1A_1$ state at an avoided configuration crossing at C_s geometries, thus allowing such emission. Theoretically, Xie et al. [23] have recently developed a near-equilibrium empirical potential energy surface for $SO_2(\tilde{C}\,^1B_2)$. The calculated resonance emission spectra agree reasonably well with experimental data for states in the red wing of the $\tilde{C} \leftarrow \tilde{X}$ absorption [20,21].

In this Letter, we report a combined experimental and theoretical study of the resonance emission spectrum of $SO_2(\tilde{C}\,^1B_2)$ just below the predissociation threshold. The state-selected emission spectra provide valuable insights into the geometric differences of the two potential energy surfaces and possibly the predissociation pathways. This Letter is organized as follows. The experimental setup (Section 2) and theoretical methods (Section 3) are first briefly outlined. The measured and calculated spectra are then compared and discussed in Section 4. The concluding remarks are given in Section 5.

2. Experimental

The instrumentation used to obtain the emission spectrum of SO_2 has been discussed previously [17,24]. The 532 nm output of a Quantel YG580-C series Nd:YAG laser operating at 20 Hz pumps a Lambda Physik FL3002E dye laser with an intracavity etalon used to reduce the bandwidth of the dye laser to 0.05 cm^{-1}. The dye used in these experiments was a mix of DCM and LDS 698 (Exciton) to generate light between 683 and 659 nm. Typically, the dye laser energies were 15 mJ per pulse. The output of the dye laser was frequency doubled in a KDP crystal (Lambda Physik FL 30) giving about 5 mJ per pulse. The 300 and 600 nm beams were frequency summed in a BBO crystal (Inrad 561-044). A Pellin–Broca prism then separated the collinear 226, 340 and 680 nm photons.

The SO_2 (Matheson) was introduced into the vacuum chamber as a free jet expansion from an IOTA ONE pulsed valve (General Valve) with an open time of 200 μs. The incident laser pulse interacted with the SO_2 molecules about 1.0 cm from the nozzle orifice.

Light scattered at 90° to the incident laser propagation direction was collected with an 4″ focal length lens and focused with an 10″ focal length lens onto the entrance slit of a spectrometer (Acton SpectraPro 275), which dispersed the light with a 2400 gr/mm grating (Milton–Roy). The dispersed light was then imaged onto an optical multichannel analyzer, OMA, (EG&G PARC 1456B-990-HQ). The spectral resolution is limited by the width of the entrance slit on the spectrometer (20 μm) and the ruling of the grating. Spectral resolution is about 25 cm^{-1} FWHM using this grating.

The varying linear dispersion across the spectrometer array was calibrated piecewise using the resonant laser line and the Hg lines at 253.6506 nm and

at 237.832 nm. The calibration of the dye laser was confirmed by the optogalvanic effect using a Mg and a Li hollow cathode lamp [25].

3. Theory

The resonance emission and Raman spectra reported here were obtained using the recently proposed Chebyshev propagation method [26]. The procedure for calculating both the resonance Raman and emission spectra can be found elsewhere [23,27]. In brief, correlation functions were first calculated in the Chebyshev order domain using the Chebyshev recursion, and then Fourier transformed to yield corresponding spectra. Following the recent work of Xie et al. [23], the three-dimensional non-rotating Hamiltonian was expressed in the Radau coordinates and the Condon approximation was invoked for the transitions. The vibrational eigenstates on an empirical ground electronic state potential energy surface were obtained in the previous work of Ma et al. [28,29].

The near-equilibrium potential energy surface of the $\tilde{C}\,^1B_2$ state of SO_2 has recently been developed by Xie et al. [23] by fitting experimental vibrational frequencies [4]. The double-well potential is consistent with previous model Hamiltonians [30,31] and gives a root-mean-squares error of 1.45 cm^{-1} for 21 low-lying vibrational frequencies [23]. Due to the strong coupling between the stretching modes, the vibrational wavefunctions show some unusual features, as discussed by several previous theoretical studies [23,31–34]. The emission spectra from four vibrational states near the bottom of the $\tilde{C}\,^1B_2$ surface have been calculated [23]. The reasonably good agreement with the experiment of Yamanouchi et al. [20,21] gave us some confidence in the empirical potential energy surface near its equilibrium position.

Since most of the vibrational levels used in the fitting are below 2500 cm^{-1} relative to the vibrational ground state, however, the accuracy of the potential energy surface is untested for moderately excited vibrational states. Furthermore, it has been shown [23] that the potential energy surface may experience difficulties for states with excited antisymmetric vibration because few levels with $n_3 > 2$ have been observed and included in the fitting.

4. Results

4.1. Experimental emission spectra

Fig. 1 displays the dispersed resonance emission spectra of SO_2 at excitation wavelengths of 227.73, 224.77, 222.92, 221.16, and 219.81 nm, with $\tilde{X}$ state vibrational assignments. The excitation wavelengths were chosen to correspond to the $\tilde{C}(1,1,0)$, $\tilde{C}(2,0,0)$, $\tilde{C}(2,1,0)$, $\tilde{C}(2,2,0)$, and $\tilde{C}(3,0,0)$ vibrational states, based on the experimental assignment of Yamanouchi et al. [4]. The spectra are best referred to as resonance emission because of the relatively long lifetimes of these vibrational states.

A number of interesting observations is noted. First, the emission spectrum strongly depends on the excitation wavelength, or more precisely on the $\tilde{C}\,^1B_2$ state vibrational quanta. This is expected since the Franck–Condon overlaps, which determine the intensity of the spectrum, are quite different for these vibrational states. Second, all the spectra are dominated by the $(n_1\nu_1, n_2\nu_2, 0)$ or simply $(n_1, n_2, 0)$ progressions. The activity in the anti-symmetric stretching mode is very weak, evidenced by only a few emission bands to states with one quantum in ν_3. (Note that all the $\tilde{C}$ state vibrational states from which emission occurs have zero quanta in ν_3). The dominance of the $(n_1, n_2, 0)$ progressions indicates that the excited state in this energy range is mainly of $^1B_2$ character.

Specifically, the spectrum at 227.73 nm ((1,1,0) excitation) is very simple and dominated by the $(n_1,0,0)$ and $(n_1,1,0)$ progressions; both peak at $n_1 = 3$ and have similar intensities. Similar progressions with higher bending quanta are also seen. At 224.77 nm ((2,0,0) excitation), there are more such progressions with $n_2 = 0–5$ and peak positions at $n_1 = 1$ or 2. The $(n_1,4,0)$ progression is the strongest and peaks at $n_1 = 2$. The spectra at 219.81 nm ((3,0,0) excitation) can also be assigned to $(n_1,n_2,0)$ progressions with $n_2 = 0–6$, with peaks at $n_1 = 1$ or 2. The spectra at 221.16 ((2,2,0) excitation) and 222.92 nm ((2,1,0) excitation) are, on the other hand, much more complex than the others, although most bands still belong to $(n_1,n_2,0)$-type progressions. The complexity is largely due to stronger emissions to states with large bending quanta (n_2 up to 11). The pat-

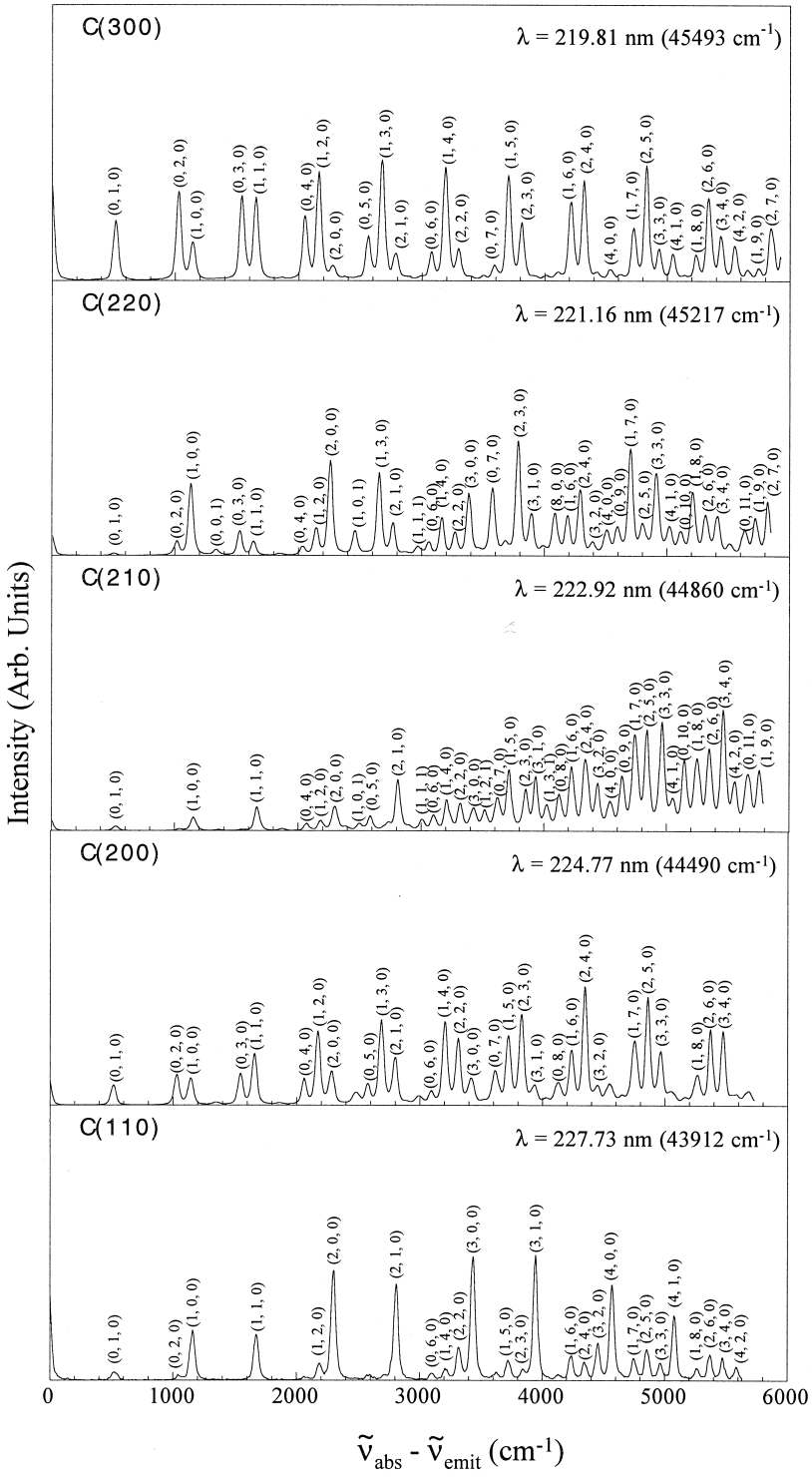

Fig. 1. Experimental dispersed resonance emission spectra of $SO_2(\tilde{C}\,^1B_2)$ at five excitation frequencies.

terns observed here are similar to those found in an earlier emission study by Yamanouchi et al. [20,21]. The activity in the symmetric stretching and bending modes can be readily understood since the $\tilde{C}\,^1B_2$ state has longer equilibrium bond lengths and a smaller equilibrium bending angle than the $\tilde{X}$ state.

4.2. Calculated emission spectra

Fig. 2 displays the emission spectra calculated for the five vibrational states of $SO_2(\tilde{C}\,^1B_2)$ excited in the experiment. Since the energies of these states on the empirical potential energy surface differ slightly from the experimental values, the excitation wavelengths are not exactly the same as in Fig. 1.

The spectra at the two lowest excitation energies reproduce the experimental data reasonably well. For the $\tilde{C}(1,1,0)$ state, for example, the calculated spectrum is dominated by the $(n_1,0,0)$ and $(n_1,1,0)$ progressions below 5000 cm^{-1}, in excellent agreement with the experimental spectrum at 227.73 nm. These two progressions are of similar intensities and peak at $n_1 = 3$, again in agreement with the experimental spectrum. The calculated spectrum has significantly higher intensities for the $(n_1,n_2,0)$ bands with $n_2 =$ 2–6 than the experimental spectrum reported here. Two peaks are present in the bending progression at $n_2 = 0$ and 5, reflecting the nodal structure of the $\tilde{C}(1,1,0)$ wavefunction in the bending coordinate. Similarly, there is an additional peak near 12 000 cm^{-1} (not shown here) owing to the nodal structure of the wavefunction in the symmetric stretching coordinate. This higher peak in the emission spectrum has been observed by Yamanouchi et al. [21], who found that the peaks in n_2 occur at 1–2 and 6–8, consistent with our calculation. These authors did not, however, mention emission in the energy range of this work.

The agreement for the higher $\tilde{C}(2,0,0)$ state is not as satisfactory, although the major features of the experimental spectrum are reproduced. For example, the progressions $(n_1,n_2,0)$ for $n_2 = 0$–5 are present in the calculated spectrum, although their intensities do not quite agree with the observation. In addition, significant intensities are found for emissions to the $n_3 = 2$ anti-symmetric stretching state in the calculated spectrum, but these emissions are absent in the experimental spectrum. The discrepancies, also found for the lower $\tilde{C}(1,0,0)$ state [23], are attributable to the inadequacy of the empirical $\tilde{C}\,^1B_2$ potential energy surface in the anti-symmetric stretching coordinate.

At higher energies, no meaningful comparison can be made between the calculated and measured spectra. We believe that this failure to reproduce the experimental spectra stems from the inaccuracy of the empirical $\tilde{C}\,^1B_2$ potential energy surface. As mentioned above, the experimental vibrational frequencies used in optimizing the potential energy surface are mostly below 2500 cm^{-1}. The energies of the $\tilde{C}(2,1,0)$, $\tilde{C}(2,2,0)$, and $\tilde{C}(3,0,0)$ states are 2285, 2644, and 2920 cm^{-1} above the ground vibrational state.

4.3. Calculated resonance Raman spectra

If the lifetime of $SO_2(\tilde{C}\,^1B_2)$ is short, the excitation/emission process becomes a coherent Raman process [35]. The resonance Raman spectrum via the $\tilde{C}\,^1B_2$ state of SO_2 has been measured in a hexane solution [22], where the solvent induced vibrational relaxation is rapid. Interestingly, no transition to vibrational levels with odd ν_3 quanta was observed in the experiment, even at a high energy (208.9 nm). In our calculation, the propagation was terminated before the excited state wavepacket recurs, which corresponds to a short stay on the excited state potential energy surface. The calculated spectra at three experimental frequencies (228.7, 223.1, and 208.9 nm) are given in Fig. 3. It can be readily seen that all the spectra are dominated by a progression in $(n_1,0,0)$, which peaks at the first overtone and decreases with n_1. These characteristics are in excellent agreement with experimental observation of Yang and Myers [22]. The dominance of the $(n_1,0,0)$ series indicates that the initial motion of the excited wavepacket is primarily in the symmetric stretching coordinate.

In contrast to the emission spectra, the Raman intensities were found insensitive to the excitation frequency. This is understandable based on the short lifetime on the excited state. Under such circumstances, the empirical $\tilde{C}\,^1B_2$ potential energy surface

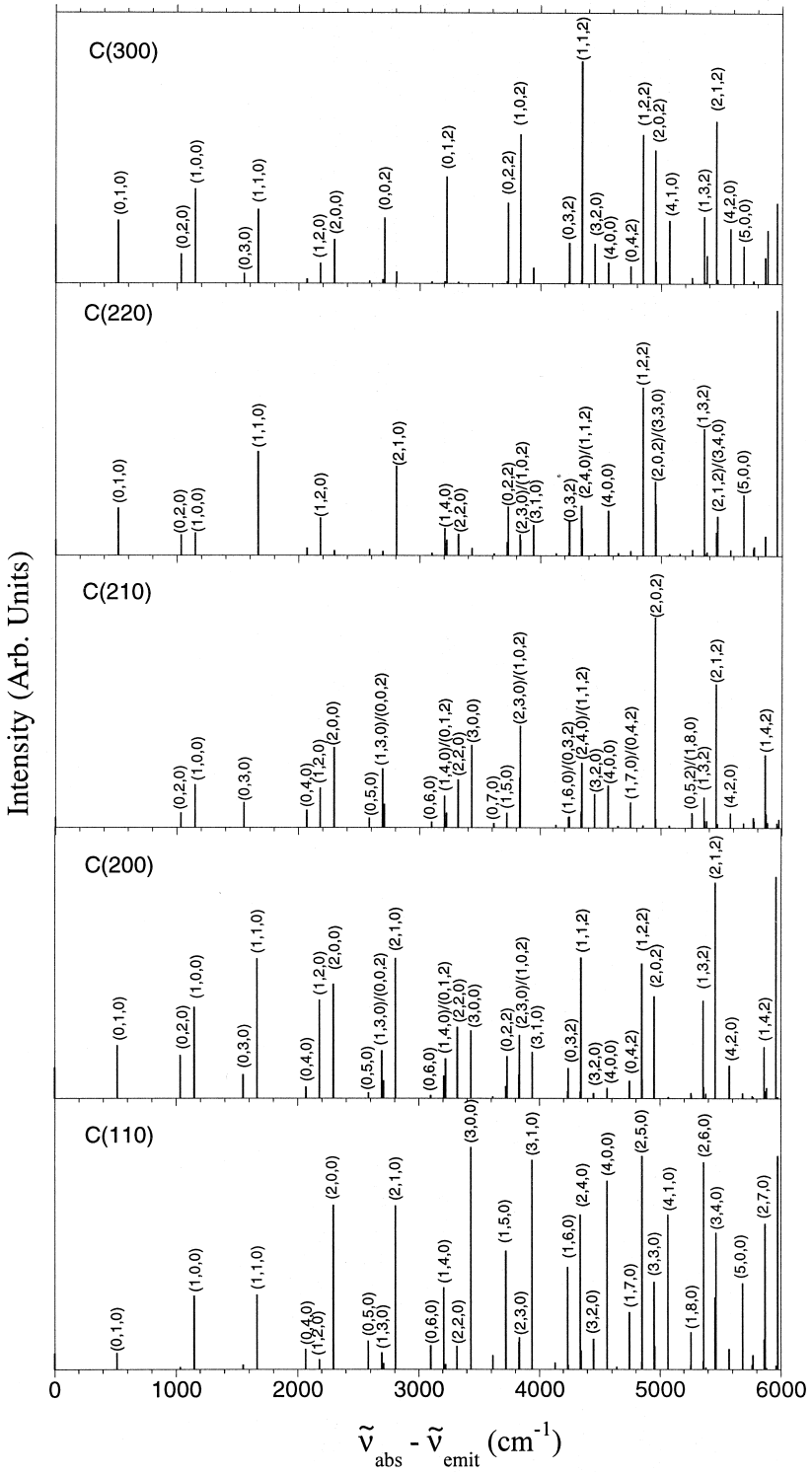
C(300)
(0,1,0)
(0,2,0)
(1,0,0)
(0,3,0)
(1,1,0)
(1,2,0)
(2,0,0)
(0,0,2)
(0,1,2)
(0,2,2)
(1,0,2)
(0,3,2)
(1,1,2)
(3,2,0)
(4,0,0)
(0,4,2)
(1,2,2)
(2,0,2)
(4,1,0)
(1,3,2)
(2,1,2)
(4,2,0)
(5,0,0)
C(220)
(0,1,0)
(0,2,0)
(1,0,0)
(1,1,0)
(1,2,0)
(2,1,0)
(1,4,0)
(2,2,0)
(0,2,2)
(2,3,0)/(1,0,2)
(3,1,0)
(0,3,2)
(2,4,0)/(1,1,2)
(4,0,0)
(1,2,2)
(2,0,2)/(3,3,0)
(1,3,2)
(2,1,2)/(3,4,0)
(5,0,0)
C(210)
(0,2,0)
(1,0,0)
(0,3,0)
(0,4,0)
(1,2,0)
(2,0,0)
(0,5,0)
(1,3,0)/(0,0,2)
(0,6,0)
(1,4,0)/(0,1,2)
(2,2,0)
(3,0,0)
(0,7,0)
(1,5,0)
(2,3,0)/(1,0,2)
(1,6,0)/(0,3,2)
(2,4,0)/(1,1,2)
(3,2,0)
(4,0,0)
(1,7,0)/(0,4,2)
(2,0,2)
(0,5,2)/(1,8,0)
(1,3,2)
(2,1,2)
(4,2,0)
(1,4,2)
C(200)
(0,1,0)
(0,2,0)
(1,0,0)
(0,3,0)
(1,1,0)
(0,4,0)
(1,2,0)
(2,0,0)
(0,5,0)
(1,3,0)/(0,0,2)
(2,1,0)
(0,6,0)
(1,4,0)/(0,1,2)
(2,2,0)
(3,0,0)
(0,2,2)
(2,3,0)/(1,0,2)
(3,1,0)
(0,3,2)
(1,1,2)
(3,2,0)
(4,0,0)
(0,4,2)
(1,2,2)
(2,0,2)
(1,3,2)
(2,1,2)
(4,2,0)
(1,4,2)
C(110)
(0,1,0)
(1,0,0)
(1,1,0)
(0,4,0)
(1,2,0)
(2,0,0)
(0,5,0)
(1,3,0)
(2,1,0)
(0,6,0)
(1,4,0)
(2,2,0)
(3,0,0)
(1,5,0)
(2,3,0)
(3,1,0)
(1,6,0)
(2,4,0)
(3,2,0)
(4,0,0)
(1,7,0)
(2,5,0)
(3,3,0)
(4,1,0)
(1,8,0)
(2,6,0)
(3,4,0)
(5,0,0)
(2,7,0)
Intensity (Arb. Units)
0
1000
2000
3000
4000
5000
6000
$\tilde{\nu}_{abs} - \tilde{\nu}_{emit}$ (cm^{-1})

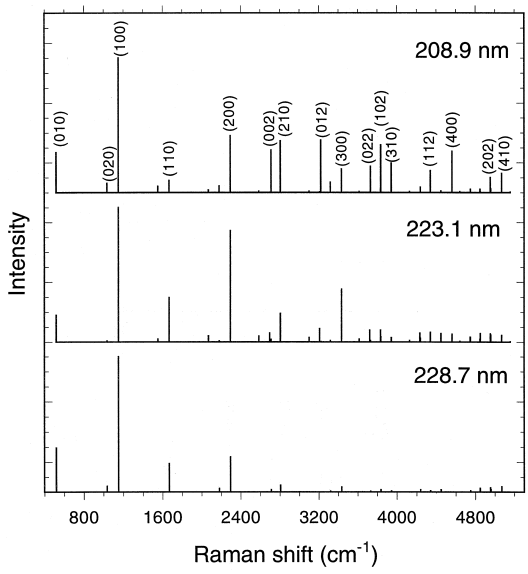

Fig. 3. Calculated resonance Raman spectra of $SO_2(\tilde{C}\,^1B_2)$ at three excitation frequencies.

is sufficient to accurately describe the resonance Raman spectrum.

5. Concluding remarks

In this work, we report experimental measurements of resonance emission spectra of five vibrational states of $SO_2(\tilde{C}\,^1B_2)$ that lie just below the predissociation threshold. These spectra are dominated by emissions to both the symmetric stretching and bending modes, although weak emissions to $n_3 = 1$ levels have also been found. The dominance of the $(n_1,n_2,0)$ progressions indicates that the excited electronic state is of predominantly $^1B_2$ character. However, the presence of emissions to levels with odd n_3, which are not observed at lower excitation energies, may signal the onset of configuration interaction mixing with a nearby electronic state at C_s geometries. The identity of this state is unclear at this moment, although mixing with the repulsive $3\,^1A_1$ state is a likely explanation for the prominent emission bands to odd n_3 levels that are observed at the near 50 000 cm^{-1} excitation [17]. For the low-lying vibrational states of the $\tilde{C}$ state excited here one cannot exclude mixing of the $\tilde{C}\,^1B_2$ state with the ground electronic state. This would be consistent with the proposed internal conversion pathway via the $\tilde{X}\,^1A_1$ state [9], which is supported by a number of recent experiments [5,6].

Theoretically, reasonably good agreement is found for emission spectra from the $\tilde{C}(1,1,0)$ and $\tilde{C}(2,0,0)$ states. For states with higher energies, however, the agreement deteriorates. This inability to reproduce experimental spectra testifies to the inadequacy of the empirical potential energy surface at higher energies, which can be attributed to the lack of data on highly excited vibrational levels for the fitting process and to possible involvement of other electronic states. Both factors affect the potential energy surface in configurations far away from the $\tilde{C} \leftarrow \tilde{X}$ Franck–Condon region. Indeed, the excellent agreement between the calculated and measured resonance Raman spectra and resonance emission spectra from low-lying vibrational states indicate that the empirical $\tilde{C}\,^1B_2$ potential energy surface is reasonably reliable in the Franck–Condon region. This work clearly demonstrates the urgent need for high quality ab initio potential energy surfaces of this system.

Note added in proof: After this Letter was sent to press, a relevant paper by Bludsky et al. [36] appeared in the literature. These authors have derived a three-dimensional potential of the $\tilde{C}\,^1B_2$ state from high-level ab initio calculations and determined the corresponding low-lying vibrational energy levels. This work strongly supports the suggestion made in Ref. [17] that a repulsive singlet state is involved in the predissociation of the $\tilde{C}\,^1B_2$ state of SO_2 at high energies.

Acknowledgements

The work at University of Chicago was supported by the Division of Chemical Sciences, Office of

Fig. 2. Calculated dispersed resonance emission spectra of $SO_2(\tilde{C}\,^1B_2)$ for five vibrational states corresponding to the five excitation frequencies.

Basic Energy Sciences, Office of Energy Research, US Department of Energy, under Grant No. DE-FG02-92ER14305. The UNM team was supported by the National Science Foundation (CHE-9713995) and in part by the National Natural Science Foundation of China (DX). We thank Prof. Yamanouchi and Dr. Katagiri for sending us the ab initio data of SO_2.

References

[1] H. Okabe, J. Am. Chem. Soc. 93 (1971) 7095.
[2] M.-H. Hui, S.A. Rice, Chem. Phys. Lett. 17 (1972) 474.
[3] T. Ebata, O. Nakazawa, M. Ito, Chem. Phys. Lett. 143 (1988) 31.
[4] K. Yamanouchi, M. Okunishi, Y. Endo, S. Tsuchiya, J. Mol. Struct. 352/353 (1995) 541.
[5] A. Okazaki, T. Ebata, N. Mikami, J. Chem. Phys. 107 (1997) 8752.
[6] H. Katagiri, T. Sako, A. Hishikawa, T. Yazaki, K. Onda, K. Yamanouchi, K. Yoshino, J. Mol. Struc. 413/414 (1997) 589.
[7] S. Becker, C. Braatz, J. Lindner, E. Tiemann, Chem. Phys. 196 (1995) 275.
[8] R. Vasudev, W.M. McClain, J. Mol. Spectrosc. 89 (1981) 125.
[9] M. Ivanco, J. Hager, W. Sharfin, S.C. Wallace, J. Chem. Phys. 78 (1983) 6531.
[10] A. Freedman, S.-C. Yang, R. Bersohn, J. Chem. Phys. 70 (1979) 5313.
[11] M. Kawasaki, K. Kasatani, H. Sato, H. Shinohara, N. Nishi, Chem. Phys. 73 (1982) 377.
[12] H. Kanamori, J.E. Butler, K. Kawaguchi, C. Yamada, E. Hirota, J. Chem. Phys. 83 (1985) 611.
[13] M. Kawasaki, H. Sato, Chem. Phys. Lett. 139 (1987) 585.
[14] P. Felder, C.S. Effenhauser, B.M. Haas, J.R. Huber, Chem. Phys. Lett. 148 (1988) 417.
[15] C. Braatz, E. Tiemann, Chem. Phys. 229 (1998) 93.
[16] K. Kamiya, H. Matsui, Bull. Chem. Soc. Jpn 64 (1991) 2792.
[17] P.C. Ray, M.F. Arendt, L.J. Butler, J. Chem. Phys. 109 (1998) 5221.
[18] P. Nachtigall, J. Hrusak, O. Bludsky, S. Iwata, J. Chem. Phys. 303 (1999) 441.
[19] J.C.D. Brand, D.R. Humphrey, A.E. Douglas, I. Zanon, Can. J. Phys. 51 (1973) 530.
[20] K. Yamanouchi, H. Yamada, S. Tsuchiya, J. Chem. Phys. 88 (1988) 4664.
[21] K. Yamanouchi, S. Takeuchi, S. Tsuchiya, J. Chem. Phys. 92 (1990) 4044.
[22] T.-S. Yang, A.B. Myers, J. Chem. Phys. 95 (1991) 6207.
[23] D. Xie, G. Ma, H. Guo, J. Chem. Phys. 111 (1999) 7782.
[24] M.F. Arendt, L.J. Butler, J. Chem. Phys. 109 (1998) 7835.
[25] D.S. King, P.K. Shenck, K.C. Smyth, J.C. Travis, Appl. Opt. 16 (1997) 2617.
[26] R. Chen, H. Guo, Comput. Phys. Comm. 119 (1999) 19.
[27] H. Guo, Chem. Phys. Lett. 289 (1998) 396.
[28] G. Ma, R. Chen, H. Guo, J. Chem. Phys. 110 (1999) 8408.
[29] G. Ma, H. Guo, J. Chem. Phys. 111 (1999) 4032.
[30] A.R. Hoy, J.C.D. Brand, Mol. Phys. 36 (1978) 1409.
[31] T. Sako, A. Hishikawa, K. Yamanouchi, Chem. Phys. Lett. 294 (1998) 571.
[32] T. Sako, K. Yamanouchi, F. Iachello, Chem. Phys. Lett. 299 (1999) 35.
[33] S.C. Farantos, Laser Chem. 13 (1993) 87.
[34] R. Prosmiti, S.C. Farantos, H.S. Taylor, Mol. Phys. 82 (1994) 1213.
[35] E.J. Heller, Acc. Chem. Res. 14 (1981) 368.
[36] O. Bludsky, P. Nachtigall, J. Hrusak, P. Jensen, Chem. Phys. Lett. 318 (2000) 607.